



ELSEVIER

Contents lists available at ScienceDirect

Journal of Marine Systems

journal homepage: www.elsevier.com/locate/jmarsys

Phytoplankton size structure in the western South China Sea under the influence of a ‘jet-eddy system’

Wenzhao Liang^{a,b,c}, Danling Tang^{a,b,*,1}, Xin Luo^c

^a Guangdong Key Laboratory of Ocean Remote Sensing (LORS), State Key Laboratory for Tropical Oceanography, South China Sea Institute of Oceanology, Chinese Academy of Sciences, Guangzhou 510301, China

^b University of Chinese Academy of Sciences, Beijing 100049, China

^c Department of Earth Sciences, The University of Hong Kong, Pokfulam Road, Hong Kong, China

ARTICLE INFO

Keywords:

Phytoplankton size structure
Coastal upwelling
Jet
Eddy
River plume

ABSTRACT

A northeastward jet in the western South China Sea (SCS) usually induces phytoplankton blooms during summertime. This jet is often sandwiched by a cyclonic eddy in the north and an anticyclonic eddy in the south. Using in situ and satellite data, the present study analyzes the combined impact of the northeastward jet and two eddies on the phytoplankton size structure (PSS) from August to September 2014. Generally, picophytoplankton is the major size fraction in surface water, contributing 73% of the total *chlorophyll a* concentration. The data showed that a high *chlorophyll a* belt (av. $0.29 \pm 0.18 \mu\text{g L}^{-1}$) with a large percentage of microphytoplankton (av. 14%) appeared in the northeastward jet. Meanwhile, similar *chlorophyll a* concentrations were observed in the cyclonic (av. $0.072 \pm 0.019 \mu\text{g L}^{-1}$) and anticyclonic eddies (av. $0.087 \pm 0.02 \mu\text{g L}^{-1}$), but microphytoplankton contributed 6.7% more in the anticyclonic eddy. Below the surface, however, the dominant size of phytoplankton switched from pico to nano and micro with increasing depth. In contrast to the observations at the surface, the jet and anticyclonic eddy presented a lower microphytoplankton contribution than the cyclonic eddy. Horizontally, advection of coastal upwelling water by the northeastward jet enhanced the growth of phytoplankton and influenced the surface PSS. Meanwhile, divergence/convergence in cyclonic/anticyclonic eddy interaction with the northeastward jet formed the high *chlorophyll a* belt at the edge of the eddy and increased the microphytoplankton contribution through water mass transport and mixing. Nutrient supply and weakening of the light intensity below the surface layer synergistically influenced the concentration and size structure of phytoplankton in the cyclonic/anticyclonic eddies at different depths. Finally, this study proposed a ‘jet-eddy system’ to explain summer spatial characteristics of PSS in the western SCS. Source water (riverine and coastal upwelling water) that feeds the ‘jet-eddy system’ is another key factor affecting phytoplankton biomass and its size structure.

1. Introduction

The ocean phytoplankton community consists of microscopic plants with a large range of body sizes, varying from picophytoplankton (0.2–2 μm) to nanophytoplankton (2–20 μm) to relatively large chains of microphytoplankton (20–200 μm). Phytoplankton size structure (PSS), as a metric of the phytoplankton community, strongly influences ecosystem functioning in aquatic environments (Irwin, 2006). Based on size specific predator–prey relations, large phytoplankton are prone to being grazed by larger zooplankton, a process that will supply food webs with high-efficiency material and energy transfer to higher trophic levels (Ryther, 1969). Both physical processes (e.g., advection

and turbulence) and environmental variables (e.g., temperature, solar radiation and nutrients) are proven to influence PSS (Li, 2002; Finkel et al., 2009; Liu et al., 2009; Chen et al., 2010). Previous field data suggest that small phytoplankton cells dominate in stable, oligotrophic environments such as the open ocean, and larger cells dominate biomass in passive and eutrophic environments such as coastal areas (Agawin et al., 2000).

Driven by the southeast monsoon, a northeastward jet is usually observed at $\sim 12^\circ\text{N}$, 110°E – 113°E with surface velocities $> 0.5 \text{ m s}^{-1}$ (Li et al., 2014), carrying cold coastal upwelling water to the South China Sea (SCS) basin (Xie et al., 2003; Kuo et al., 2000). Due to strong density stratification, the surface water in most areas of the SCS is

* Corresponding author at: Guangdong Key Laboratory of Ocean Remote Sensing (LORS), State Key Laboratory for Tropical Oceanography, South China Sea Institute of Oceanology, Chinese Academy of Sciences, Guangzhou 510301, China.

E-mail address: lingzistdl@126.com (D. Tang).

¹ <http://lingzis.51.net/>.

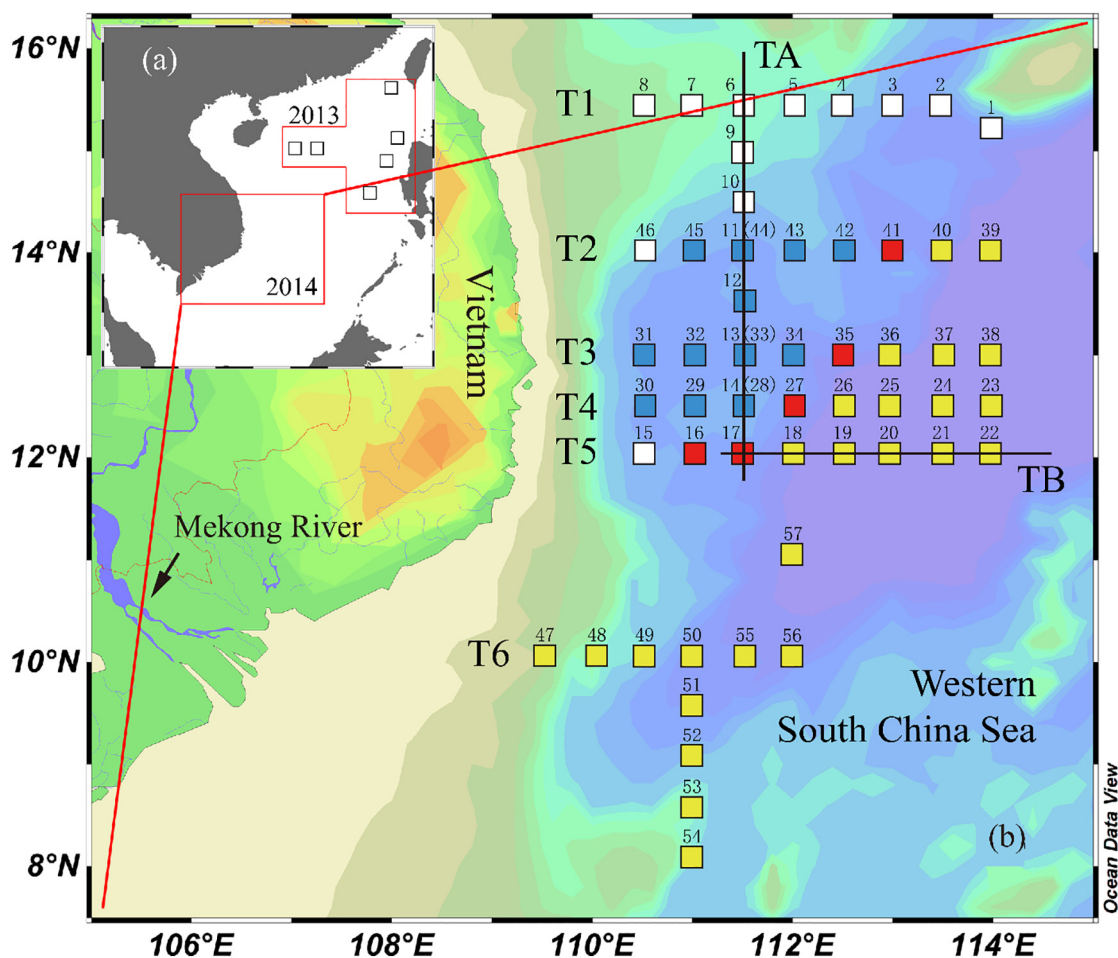


Fig. 1. (a) The geographic location of the sampling regions in the South China Sea. (b) Location of sampling stations and transects in the west South China Sea between August 29 and September 27, 2014. Squares in blue, red and yellow represented stations in cyclonic eddy, northeastward jet and anticyclonic eddy respectively. (For interpretation of the references to color in this figure legend, the reader is referred to the web version of this article.)

oligotrophic, leading to low surface phytoplankton biomass (Ning et al., 2004). Therefore, physical processes such as coastal upwelling and diffusion, control nutrient injections into the euphotic zone and play a profound role in phytoplankton growth and distribution (Cloern, 1996; McGillicuddy et al., 2003). A conceptual model of the ‘wind-pump effect’ is defined as a series of processes driven by wind that influences ocean currents and water movement and subsequently affects the ocean’s ecological status (Tang et al., 2004a; Tang et al., 2004b). It well explains a jet-shaped phytoplankton patchiness that frequently appears in the western SCS in summertime. Wind pumping is expected to change the transport of nutrients, promote the cycling of major elements in the ocean, and drive the primary production of marine ecosystems affecting carbon fixation and global fishery resources (Tang et al., 2006; Ye et al., 2017). In the same region, an offshore high *chlorophyll a* concentration area is observed in the northern jet (Tang et al., 2004a). However, this conceptual model did not explain the formation of the elevated *chlorophyll a* concentration area. To better understand this, more physical processes, especially vertical motion, should be taken into consideration.

Due to the vorticity transport derived from the nonlinear effect of the western boundary current, a dipole structure in the summertime western SCS is usually developed with a cyclonic eddy in the north and anticyclonic eddy in the south, sandwiching the northeastward jet in between, (Wang et al., 2006; Gan and Qu, 2008). Upward velocities were observed around the center of the cyclonic eddy (Hu et al., 2011). Upwelling in the cyclonic eddy injects nutrients into the euphotic zone and enhances the phytoplankton biomass (Vaillancourt et al., 2003; Lin

et al., 2010). The high *chlorophyll a* area in the north of the jet was occupied by a cyclonic eddy for more than two weeks. Was it induced by the cyclonic eddy? Meanwhile, the biological responses in the anticyclonic eddy are also complicated (Huang et al., 2010). Zhong et al. (2013) reported enhanced biomass in the anticyclonic eddy with a decreasing contribution of *Haptophytes*, but an increasing contribution of *Synechococcus* and *Prochlorococcus*. How are these changes related to the eddies?

The marine ecosystem is mediated by both jets and eddies. How do these physical processes influence the spatial characteristic of PSS? To answer these questions, we analyzed in situ and satellite data, based on which a jet and two associated eddies or namely, a ‘jet-eddy system’ is proposed to depict the joint impact of this ‘jet-eddy system’ on phytoplankton biomass and its size structure in the summertime western SCS.

2. Study region, data and methods

2.1. Sampling and analysis

The SCS is the largest marginal sea in southeastern Asia and plays an important role in regulating regional climate. The Asian monsoon has significant influence on hydrological features and the general water circulation in this region. The southwest monsoon first appears in May, expands to the entire SCS during July and August, and lasts until late September (Shaw and Chao, 1994).

The study area is situated in eastern Vietnamese coastal waters and the adjacent western SCS (Fig. 1a). The Mekong River, emptying water

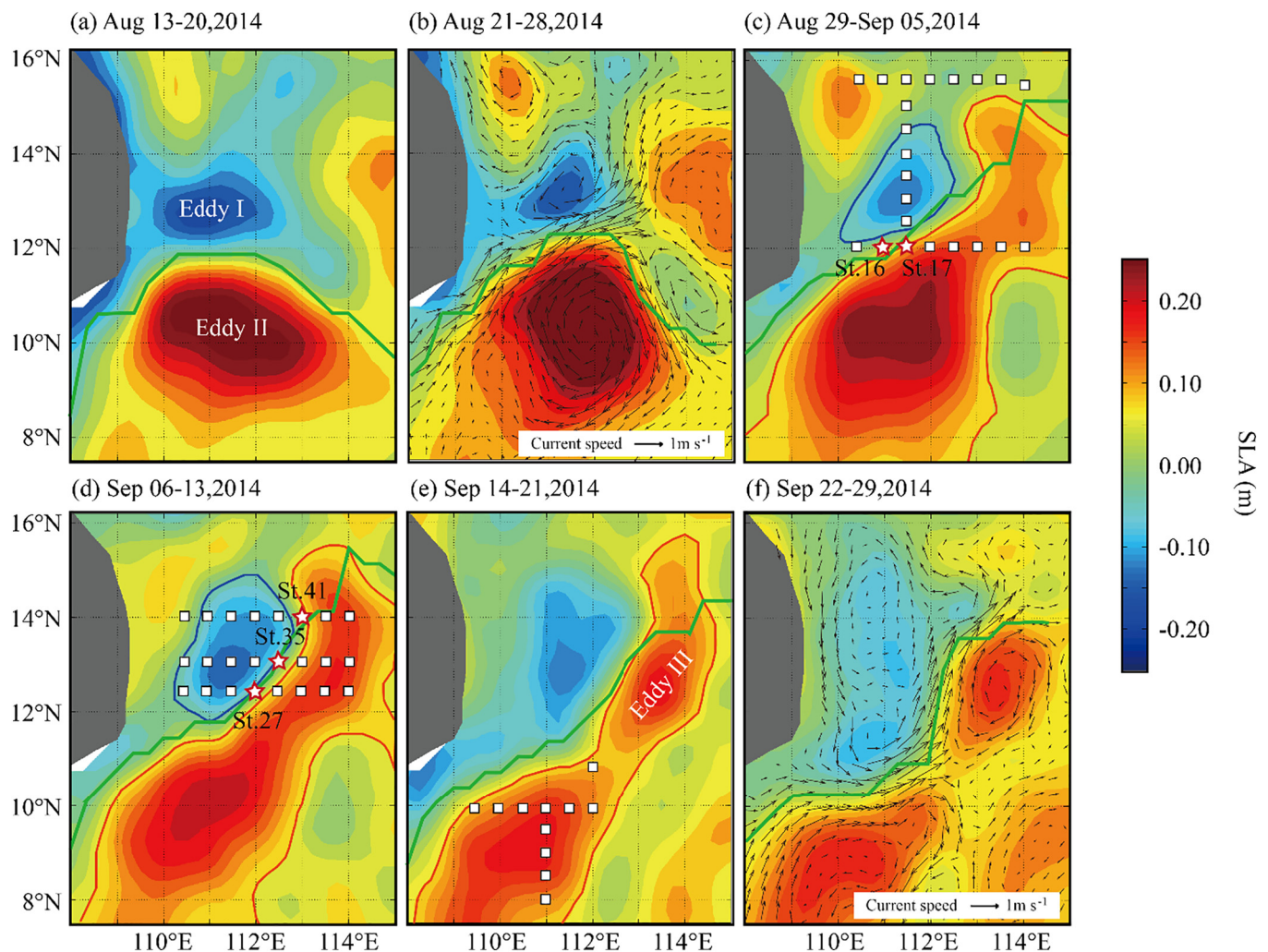


Fig. 2. Sea level anomaly during (a) August 13–20, (b) August 21–28, (c) August 29–September 5, (d) September 6–13, (e) September 14–21 and (f) September 22–29. (b) and (f) merged with sea surface current within the period. Green lines were the main axis of northeastward jet. Blue and red line in (c), (d) and (e) represented boundary of cyclonic eddy (SLA = -0.025 m) and anti-cyclonic eddy (SLA = 0.025 m). Squares and stars represented sample stations and stations in northeastward jet. (For interpretation of the references to color in this figure legend, the reader is referred to the web version of this article.)

into the SCS between 9.0°N and 10°N , is the largest river draining into the SCS with a mean annual discharge of 470 km^3 (Dagg et al., 2004). Voss et al. (2006) used the criterion of salinity < 33.2 psu to represent the Mekong River influenced area in the western SCS. Using a simple two-end-member mixing model based on the $^{228}\text{Ra}/^{226}\text{Ra}$ activity ratio and salinity, the Mekong river plume was estimated to contribute up to 53% of the surface water (0–5 m) in the western SCS water in the summertime (Chen et al., 2010). The plume changes its flow direction southward in winter and northward in summer in response to the monsoon winds (Hu et al., 2000).

2.2. Satellite and model data

Sea surface *chlorophyll a* concentration (monthly composites with 4 km resolution) and euphotic depths were derived from the Moderate Resolution Imaging Spectroradiometer (MODIS) data onboard the NASA Aqua satellite that was launched in 1999. The data were downloaded from the Distributed Active Archive Centre (DAAC) of NASA (<http://oceancol-or.gsfc.nasa.gov>). Sea level anomaly (SLA) data, merged from the radar altimeters onboard the ERS1/2, TOPEX/Poseidon, and Jason satellites, were downloaded from the AVISO website (<http://www.aviso.oceanobs.com>). Sea surface currents for specific periods of sampling were retrieved from NOAA Ocean Surface

Current Real-Time Analysis (http://www.oscar.noaa.gov/datadisplay/oscar_location.php). To better clarify physical oceanographic properties, vorticity (ω) in multilevels was calculated using the following formula: $\omega = \partial v/\partial x - \partial u/\partial y$, where (u, v) are the horizontal velocity components with positive values directed eastward (x) and northward (y), respectively. These horizontal velocity data were averaged in the sampling period and produced by the hybrid coordinate ocean model (HYCOM, <https://hycom.org/dataserver>).

2.3. In situ data

The research cruises were organized by the South China Sea Institute of Oceanology, Chinese Academy of Sciences. In situ observations were made on the cruise of western South China Sea from 27 August to 27 September 2014 at 57 sampling stations including six cross-shore transects (marked as T1 to T6 in Fig. 1). As the jet and eddies were developed in September 2013, observations of six stations from the northern SCS were used to represent the region without the influence of the jet or eddies. Profiles of temperature and salinity were obtained with Sea-Bird SBE9 Conductivity–Temperature–Depth (CTD) measurements. Seawater samples were collected with Niskin bottles triggered at seven depths (0, 25, 50, 75, 100, 150 and 200 m). One-liter samples of seawater from transects A (TA) and B (TB) at all depths were

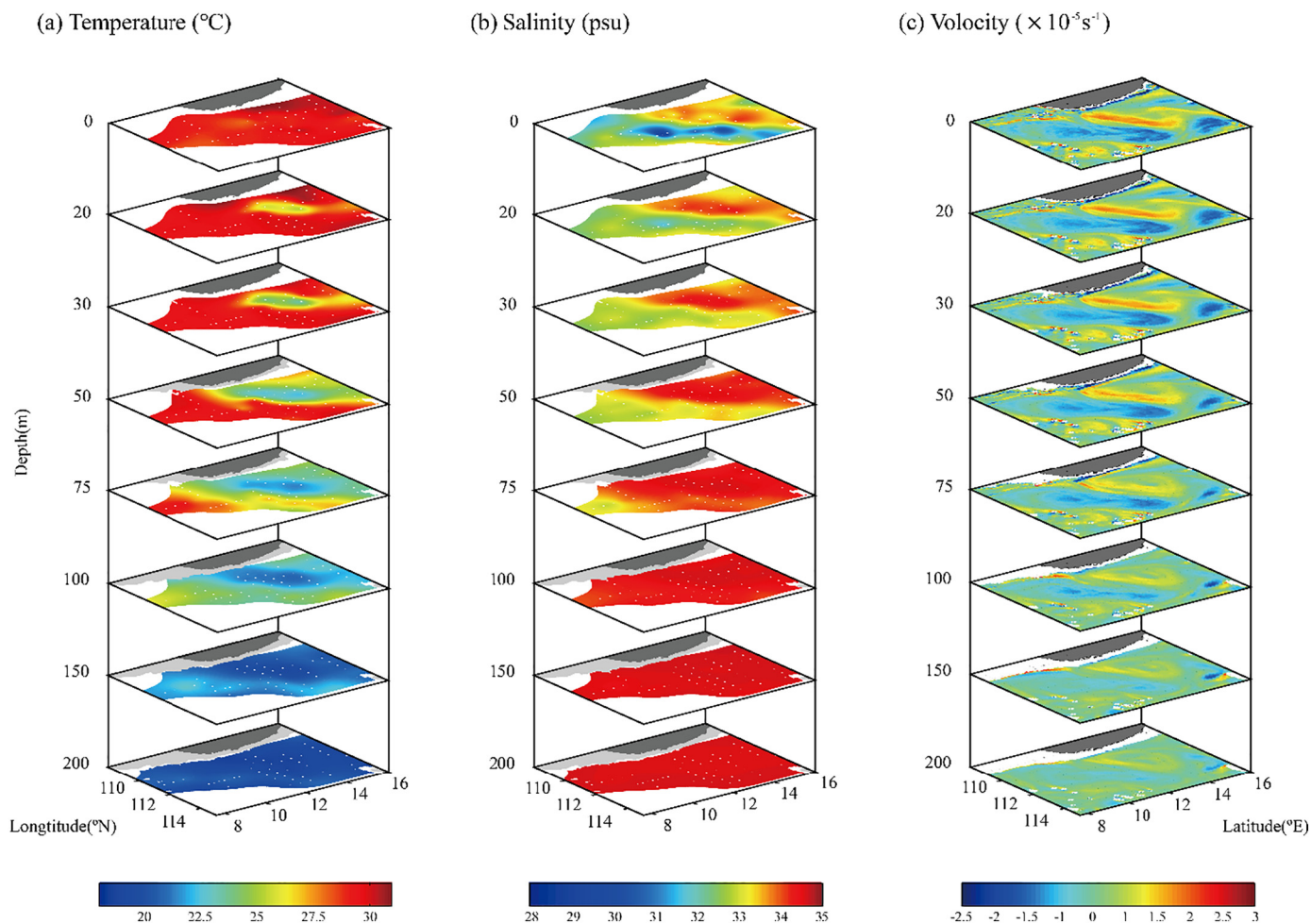


Fig. 3. Three-dimensional structure of (a) temperature, (b) salinity and (c) vorticity at the depths of 0 m, 20 m, 30 m, 50 m, 75 m, 100 m, 150 m and 200 m.

filtered through a GF/F filter (Whatman, 25 mm) for the total *chlorophyll a* concentration analysis, while 50 mL of the filtered water was collected for nutrient analysis. Two liters of seawater for PSS detection was filtered through different pore size Millipore filters (0.2, 2.0 and 20 μm). PSS measurements were made in surface water for all stations and at seven depths for 4 stations (St.1, 24, 27 and 30), as well as the 2013 stations. Filters were wrapped in aluminum foil and stored with nutrient samples in dark at -20°C before analysis. The filters were extracted with 10 mL ice-cold 90% v/v acetone in dark for 24 h. Fluorescence in the supernatant was measured by a Turner Designs TD-700 fluorometer with a 436 nm excitation filter and 680 nm emission filter. The detection limit of the Turner Designs TD-700 for *chlorophyll a* concentration is $0.01 \mu\text{g L}^{-1}$. Considering the concentration coefficient, the limit for *chlorophyll a* concentration of sample is $0.001 \mu\text{g L}^{-1}$. Concentrations of nitrate + nitrite (NO_x) and phosphate (PO_4) were analyzed on a flow injection analyzer (FIA) (Lachat Instruments, USA), using the standard pink azo dye and phosphorus molybdenum blue methods, respectively. The detection limits for NO_x and PO_4 are $0.01 \mu\text{mol L}^{-1}$ and $0.02 \mu\text{mol L}^{-1}$, respectively.

3. Results

3.1. Physical and biogeochemical observations

3.1.1. The geostrophic current field and associated eddies

SLA images showed a dipole recirculation pattern with a cyclonic cold eddy (Eddy I) in the north and an anticyclonic eddy (Eddy II) in the south (Fig. 2a). The cyclonic eddy was centered along 13°N and its

deepest SLA point was -0.2 m . From late August, as Eddies I and II weakened, an anticyclonic eddy (Eddy III) was separated from Eddy II in the northeast (Fig. 2b–e).

The northeastward jet, with a horizontal velocity of up to 1.0 m s^{-1} , was associated with the front between the cyclonic and anticyclonic eddies (Fig. 2). To identify the jet path, we define the jet axis, according to Li et al. (2014), as the meridional maximum of eastward velocity between 8°N and 16°N with a magnitude exceeding 0.1 m s^{-1} (Fig. 2). Moreover, we use SLA between -0.025 m and 0.025 m as the influenced areas of the cyclonic and anticyclonic eddies, similar to the definition in a previous study (Sun et al., 2014). Then, stations 16, 17, 27, 35 and 41 were reasonably used to represent jet stations (Fig. 2). The current was weak in both the north and south sides of the jet (Fig. 2). T1 was off the influence radius of the jet and eddies, TA crossed the center of Eddy I, and T5 was located at the area with the strongest current (Fig. 2b–c). Specifically, sampling transects of T2–T4 exactly crossed Eddy I, Eddy III and the northeastward jet (Fig. 2d). T6 was fully located in Eddy II (Fig. 2).

3.1.2. Temperature, salinity and vorticity fields

A CTD cast was conducted at a spatial interval of 50–60 km. Temperature and salinity distributions in five depths of the upper 100 m are shown in Fig. 3. The surface layer (depth = 0 m) of the study area was covered with nearly homogeneous warm water (Fig. 3). An eddy shaped isotherm formed at 25 m depth in the north, centered at 111°E , 13°N (Fig. 3). Temperatures $< 25^\circ\text{C}$ enclosed a cold core with temperature about 3°C lower than the surrounding water (Fig. 3a). At 50 m, the cold area expanded and the cold core temperature was over

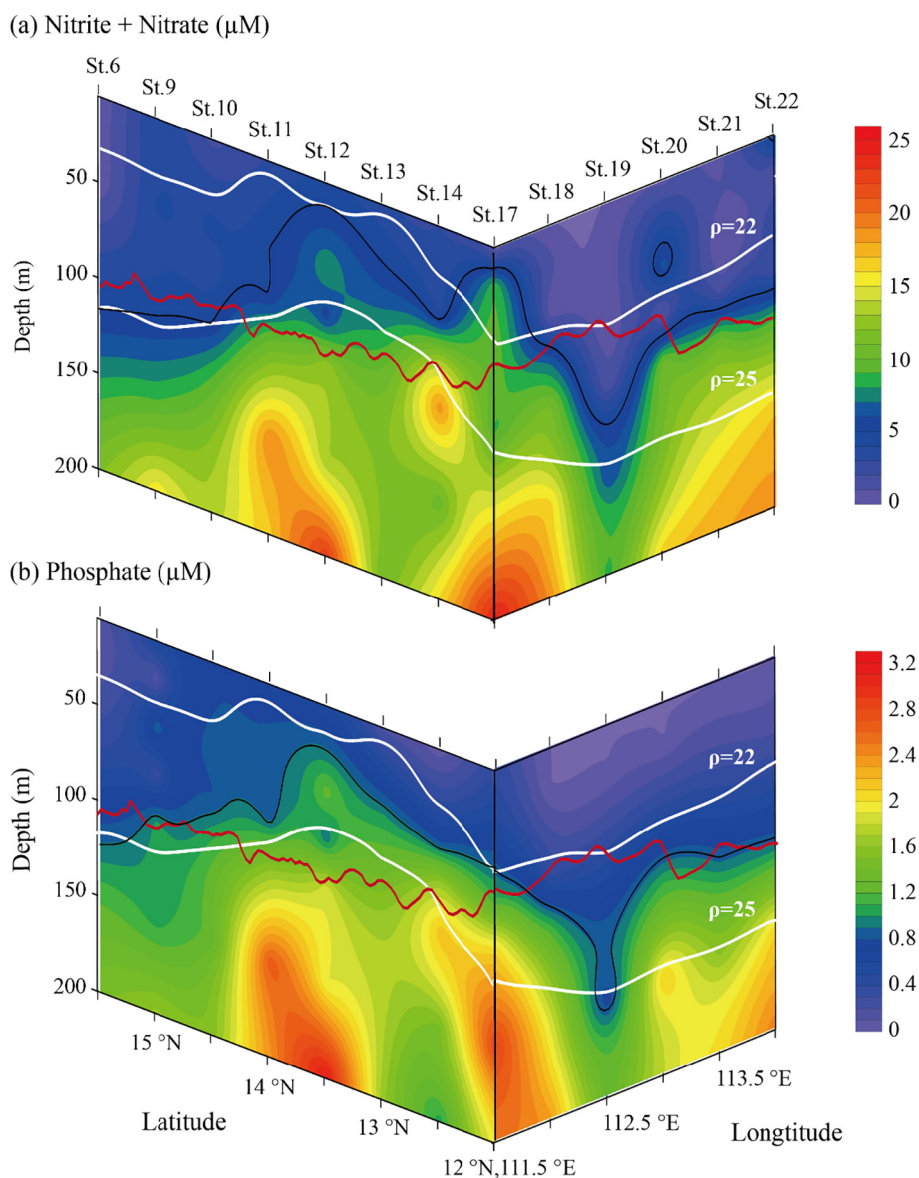


Fig. 4. The vertical distribution of (a) nitrite + nitrate and (b) phosphate in upper 200 m along 111.5°E (TA) and 12°N (TB). White lines represented density of 22 kg m^{-3} and 25 kg m^{-3} , while red lines were the euphotic depth. (For interpretation of the references to color in this figure legend, the reader is referred to the web version of this article.)

8°C lower than the surrounding water (Fig. 3a). The temperature at 75 m and 100 m decreased to approximately 18°C and the horizontal gradient was weaker below (Fig. 3a).

Less saline water was observed in the Mekong river plume, indicating dilution with terrestrial runoff (Fig. 3b). In the surface layer, low-salinity water occupied the southern part, where anticyclonic eddy was located (Fig. 3b). A strong salinity front, with a gradient $> 1.5 \text{ psu}/100 \text{ km}$, emerged from $\sim 11^\circ\text{N}$ in the coastal area and extended northeastward (Fig. 3b). At 25 m, high salinity water ($> 34 \text{ psu}$) was observed at the location of the low-temperature center (Fig. 3b). Vertically, low salinity water ($< 33.5 \text{ psu}$) extended to 75 m depth, and disappeared beneath 100 m (Fig. 3b).

The vorticity distribution showed a consistent dipole pattern at each depth throughout the water column (Fig. 3c). The maximum positive vorticity was observed in the north, indicating upwelling in the cyclonic eddy area (Fig. 3c). It decreased sharply from $> 2.0 \times 10^{-5} \text{ s}^{-1}$ at the surface to $< 1 \times 10^{-5} \text{ s}^{-1}$ at 100 m, but more gently below. Meanwhile, there was a negative vorticity to the southeast of the positive vorticity in the water column, representing the down-welling warm

eddy (Fig. 3c). Moreover, a small region along the coast with positive vorticity demonstrated an on-going coastal upwelling in the Mekong river mouth (Fig. 3c), which may be overlooked due to limited in situ data.

3.1.3. Nutrient distribution in transects A and B

Transect A (111.5°E) and transect B (12°N) crossed both the cyclonic (Eddy I) and anticyclonic eddies (Eddy III) and were characterized by the strongest influence of the northeastward jet. Both NO_x and PO_4 were nearly undetectable in surface water (Fig. 4). In subsurface layers, the $5 \mu\text{mol L}^{-1}$ of NO_x and $0.9 \mu\text{mol L}^{-1}$ of PO_4 contour shoaled up to $\sim 25 \text{ m}$ from station 11 to station 13, where a dome structure (white lines in Fig. 4), indicated by an upwelling of subsurface high density water into the euphotic layer, was also observed. However, east of station 18 (12°N , 112°E), low density water extended to a depth of 75 m, and the $5 \mu\text{mol L}^{-1}$ of NO_x and $0.9 \mu\text{mol L}^{-1}$ of PO_4 contours moved downward to a depth of 80 m (Fig. 4).

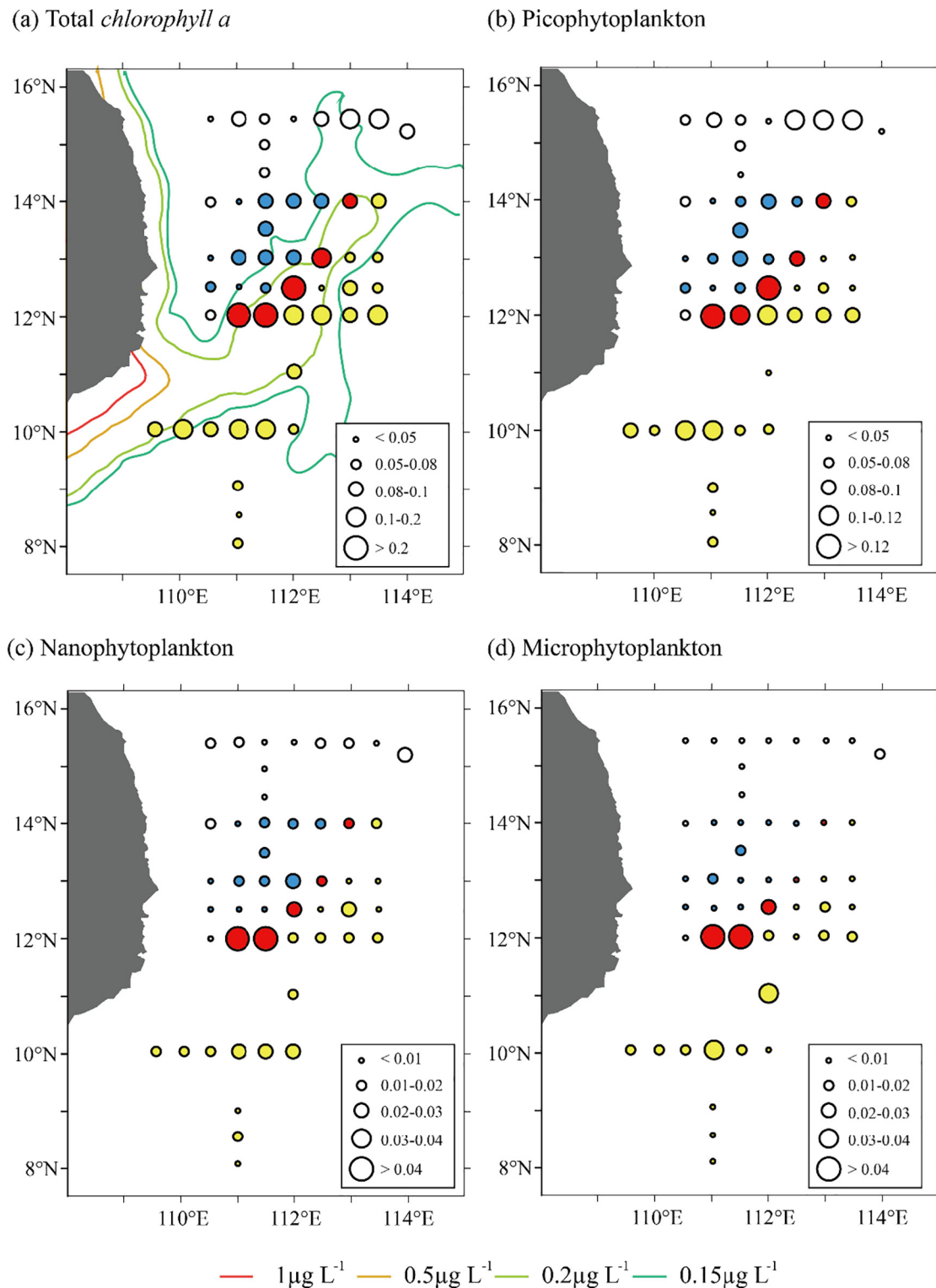


Fig. 5. Surface concentration of (a) total *chlorophyll a* (in-situ data in dot chart merged with MODIS monthly average *chlorophyll a* image), (b) picophytoplankton, (c) nanophytoplankton, and (d) microphytoplankton. (CI = $\mu\text{g L}^{-1}$). (For interpretation of the references to color in this figure, the reader is referred to the web version of this article.)

3.2. Phytoplankton biomass and size structure

3.2.1. Surface distribution

The monthly averaged MODIS *chlorophyll a* concentrations in September 2014, revealed variations of phytoplankton distribution off the eastern coast of Vietnam (Fig. 5). High *chlorophyll a* concentrations

($> 1 \mu\text{g L}^{-1}$) were observed on the coast at $\sim 11^\circ\text{N}$. A jet-shaped banding of phytoplankton biomass was formed from the Vietnamese coast to the western SCS (red filled circles in Fig. 5a). In situ observations showed that the jet stations (av. $0.29 \pm 0.18 \mu\text{g L}^{-1}$) had higher *chlorophyll a* concentration than the cyclonic (av. $0.072 \pm 0.019 \mu\text{g L}^{-1}$) and anticyclonic eddies (av.

Table 1
Parameters on surface of different area in western SCS.

Parameter	Cyclonic eddy	Jet	Anti-cyclonic eddy	OUT
Temperature (°C)	29.45 ± 0.53	28.70 ± 0.43	29.26 ± 0.41	29.74 ± 0.66
Salinity	33.60 ± 0.47	32.86 ± 0.12	31.93 ± 1.22	33.22 ± 0.37
Total Chlorophyll a (µg L ⁻¹)	0.072 ± 0.019	0.29 ± 0.18	0.087 ± 0.02	0.087 ± 0.031
Pico concentration (µg L ⁻¹)	0.063 ± 0.019	0.117 ± 0.031	0.066 ± 0.021	0.082 ± 0.032
Nano concentration (µg L ⁻¹)	0.010 ± 0.004	0.063 ± 0.060	0.015 ± 0.006	0.013 ± 0.007
Micro concentration (µg L ⁻¹)	0.003 ± 0.002	0.046 ± 0.042	0.011 ± 0.009	0.002 ± 0.001
Number of stations	N = 17	N = 5	N = 21	N = 8

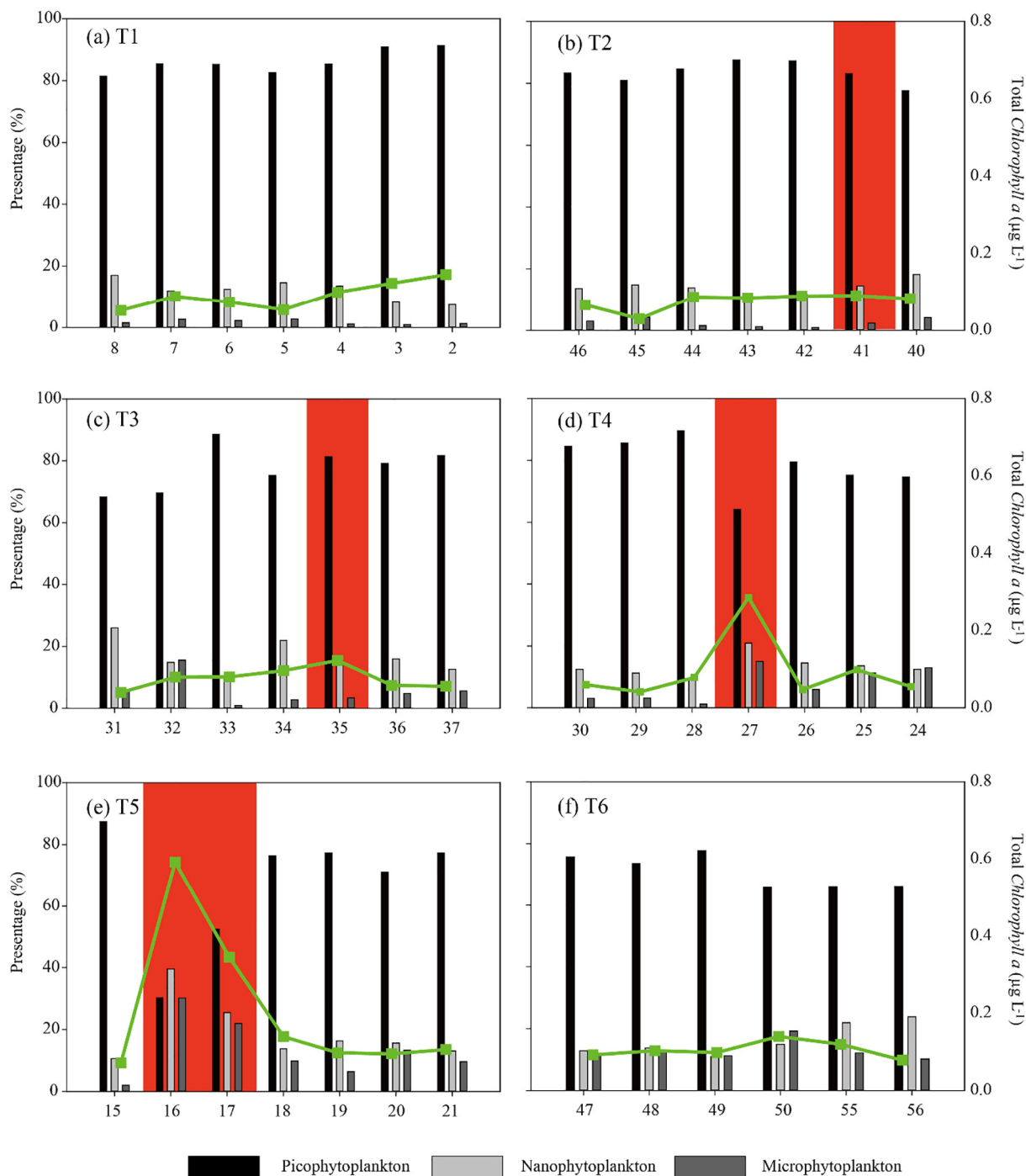


Fig. 6. Contribution of three size fractions of phytoplankton to the total chlorophyll (bar chart) and total chlorophyll a concentration (green line) in surface of (a) T1, (b) T2, (c) T3, (d) T4, (e) T5 and (f) T6. Stations with red background were located on northeastward jet. (For interpretation of the references to color in this figure legend, the reader is referred to the web version of this article.)

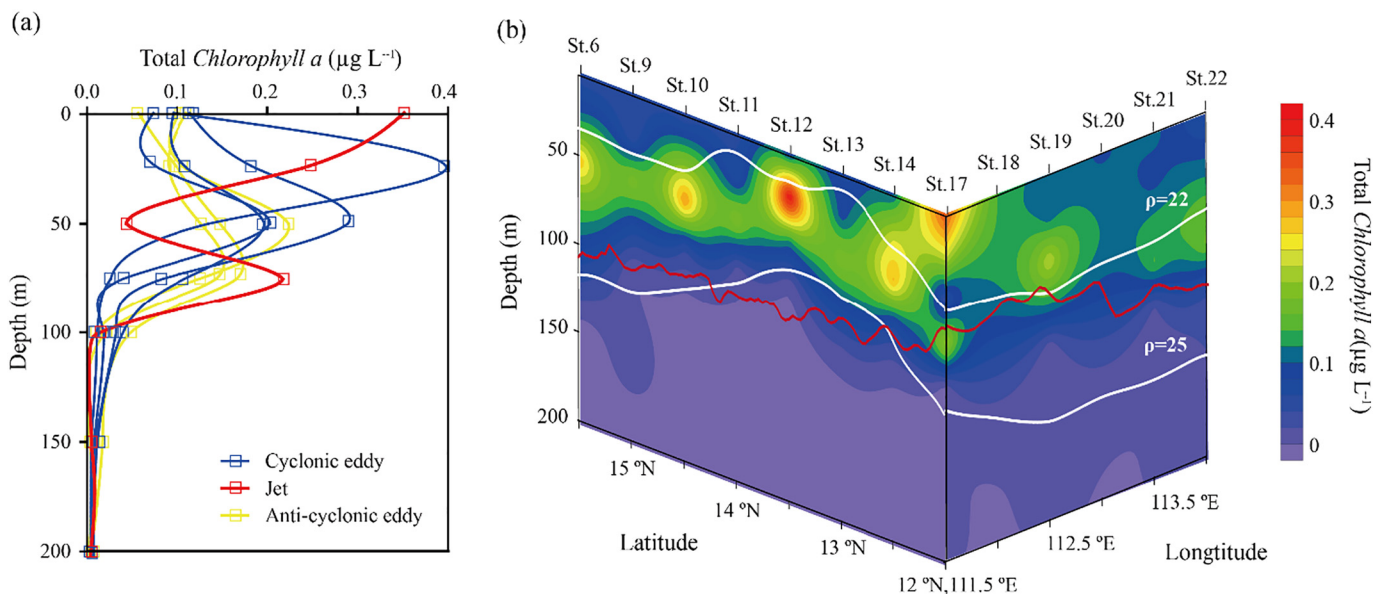


Fig. 7. (a) Vertical *chlorophyll a* concentration of stations in cyclonic eddy (station 11, 12, 13 and 14), northeastward jet (station 17), and anti-cyclonic eddy (station 18, 20 and 22) ($Cl = \mu\text{g L}^{-1}$) in transects TA and TB. (b) Vertical distribution of *chlorophyll a* in upper 200 m at transects TA and TB. White lines represented density of 22 kg m^{-3} and 25 kg m^{-3} , while red lines were the euphotic depth. (For interpretation of the references to color in this figure legend, the reader is referred to the web version of this article.)

Table 2
Three size phytoplankton concentration at depths of different area in western SCS ($\mu\text{g L}^{-1}$).

Depth	Cyclonic eddy (St.30)			Jet (St.27)			Anti-cyclonic eddy (St.24)			OUT (St.1)		
	Pico	Nano	Micro	Pico	Nano	Micro	Pico	Nano	Micro	Pico	Nano	Micro
0	0.051	0.007	0.002	0.115	0.041	0.044	0.046	0.008	0.008	0.036	0.015	0.008
25	0.030	0.014	0.003	0.292	0.055	0.023	0.076	0.009	0.002	0.015	0.008	0.002
50	0.186	0.046	0.049	0.121	0.028	0.014	0.172	0.015	0.006	0.041	0.011	0.005
75	0.052	0.017	0.013	0.017	0.013	0.002	0.075	0.019	0.010	0.070	0.018	0.007
100	0.013	0.016	0.008	0.006	0.003	0.002	0.046	0.011	0.003	0.033	0.008	< 0.001
150	0.002	0.007	0.005	0.002	0.002	0.001	0.008	0.006	0.002	0.004	0.003	< 0.001
200	0.001	0.001	0.003	0.001	< 0.001	< 0.001	< 0.001	0.002	< 0.001	0.002	0.002	< 0.001

$0.087 \pm 0.02 \mu\text{g L}^{-1}$ (Table 1). *Chlorophyll a* at station 16 was $0.59 \mu\text{g L}^{-1}$, approximately 6 times the average of the eddy areas. *Chlorophyll a* concentrations in the jet area decreased from $0.59 \mu\text{g L}^{-1}$ to $0.09 \mu\text{g L}^{-1}$.

Among all the phytoplankton community, picophytoplankton (av. $0.072 \pm 0.032 \mu\text{g L}^{-1}$) was predominant, related to nanophytoplankton (av. $0.018 \pm 0.013 \mu\text{g L}^{-1}$) and microphytoplankton (av. $0.010 \pm 0.009 \mu\text{g L}^{-1}$) in the surface water. Phytoplankton of all sizes showed higher concentrations in the jet area (Table 1). The concentration difference of picophytoplankton between the cyclonic and anticyclonic eddies was similar to nanophytoplankton. However, microphytoplankton had a large difference between the cyclonic (av. $0.003 \pm 0.002 \mu\text{g L}^{-1}$) and anticyclonic eddies (av. $0.011 \pm 0.009 \mu\text{g L}^{-1}$) (Table 1).

To look into the contribution of different size phytoplankton to total phytoplankton biomass in different areas, the percentages of different sizes for stations in six horizontal transects were compared. Picophytoplankton dominated in all stations (av. 73%) except for station 16 where the *chlorophyll a* concentration had its peak value but picophytoplankton had the lowest value (Fig. 6). Microphytoplankton had the highest average contribution in the jet stations and it decreased as the *chlorophyll a* concentration was reduced. The average microphytoplankton percentage was 10.3% in the anticyclonic eddy but was limited to 3.6% and 2.1% in the cyclonic eddy and the out of the jet-eddy area (Fig. 5). However, station 32 (111°E , 13°N), located in the center of the cyclonic eddy, showed an especially high

microphytoplankton percentage of 15.6% (Fig. 5c).

3.2.2. Vertical distribution

The vertical distribution of phytoplankton biomass in the upper 200 m was obtained in transects A (111.5°E) and B (12°N) (Fig. 7a). On the jet path, station 17 exhibited higher *chlorophyll a* concentration on the surface and declined with depth. The maximum *chlorophyll a* concentrations were mainly observed at a depth of 50 m in both the cyclonic and anticyclonic eddies, except for station 12 with a maximum level at 25 m in the center of the cyclonic eddy and stations 21 and 22 with a maximum level at 75 m in the anticyclonic eddy (Fig. 7b).

Phytoplankton biomasses with different sizes were detected at different depths for stations 1, 24, 27 and 30, representing the areas out of the jet-eddy influence, the anticyclonic eddy, the northeastward jet and the cyclonic eddy area, respectively. Picophytoplankton together with nanophytoplankton took up over 50% of the total phytoplankton biomass irrespective of the depth and location. However, a high microphytoplankton concentration was observed in the upper 25 m at station 27, which was over 4 times larger than that of stations 24 and 30 (Table 2). Meanwhile, a sharp increase in microphytoplankton was observed at 50 m depth for station 30 (Table 2).

Consequently, a noticeably high percentage of microphytoplankton was evident in the surface water of station 27 (Fig. 8b) and at 50 m for station 30 (Fig. 8a). The contribution of microphytoplankton to the *chlorophyll a* biomass in station 27 reached up to 20% in the euphotic column (Fig. 8a). Conversely, the contribution of smaller size

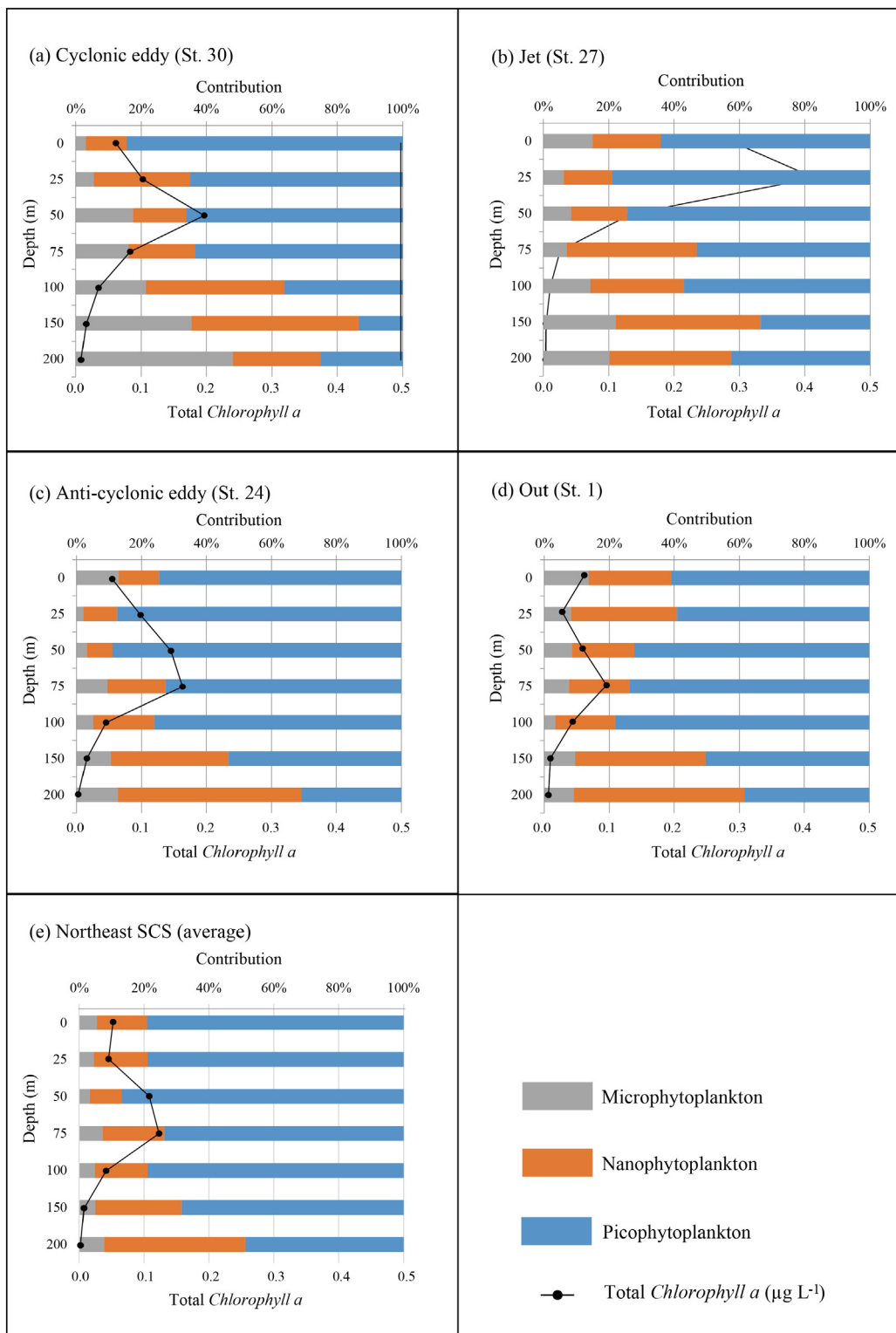


Fig. 8. Vertical distributions of *chlorophyll a* concentration and contribution of different size fractions of phytoplankton in the upper 200 m at (a) cyclonic eddy, (b) jet, (c) anti-cyclonic eddy, (d) out, and (e) average of northeastern SCS.

phytoplankton was approximately 90% of the total chlorophyll biomass at deeper levels in station 24 (Fig. 8c). Although the contribution of microphytoplankton was low beneath station 24, a comparatively higher percentage (13%) was observed on the surface than at station 30 (Fig. 7a and c).

4. Discussion

4.1. Jet-eddy system induced variations of biological and chemical properties

In the offshore region, high surface *chlorophyll a* concentration showed in a jet shaped patchiness (Fig. 5). The transport of coastal

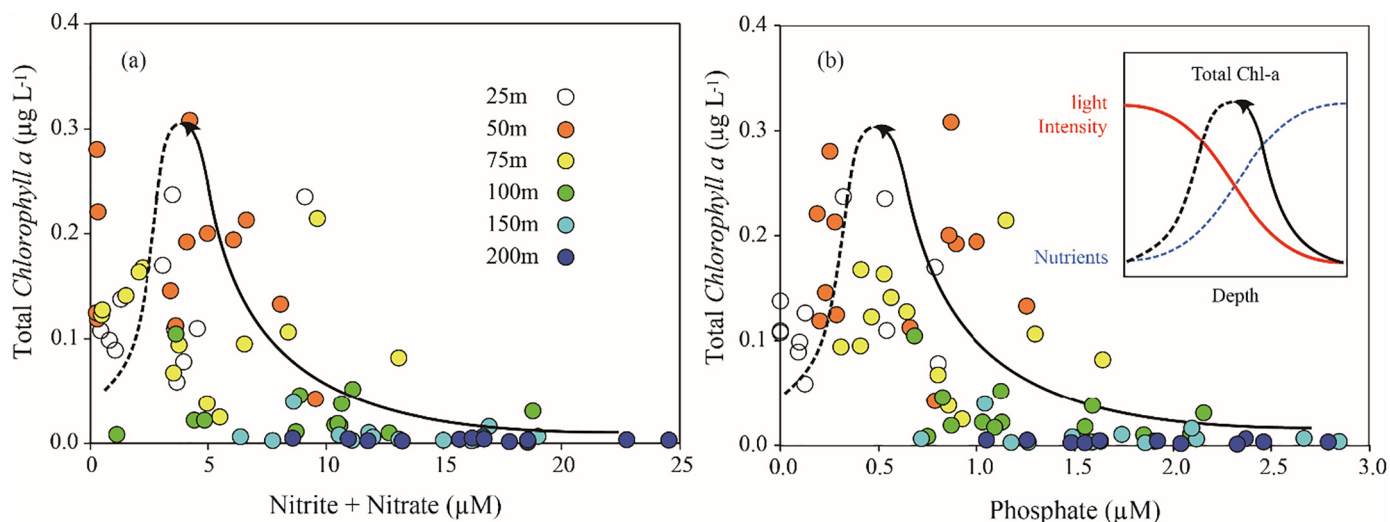


Fig. 9. The relations between nutrients (a) Nitrite + Nitrate versus-, and (b) Phosphate) versus- total chlorophyll a concentration in subsurface layer of upper 200 m.

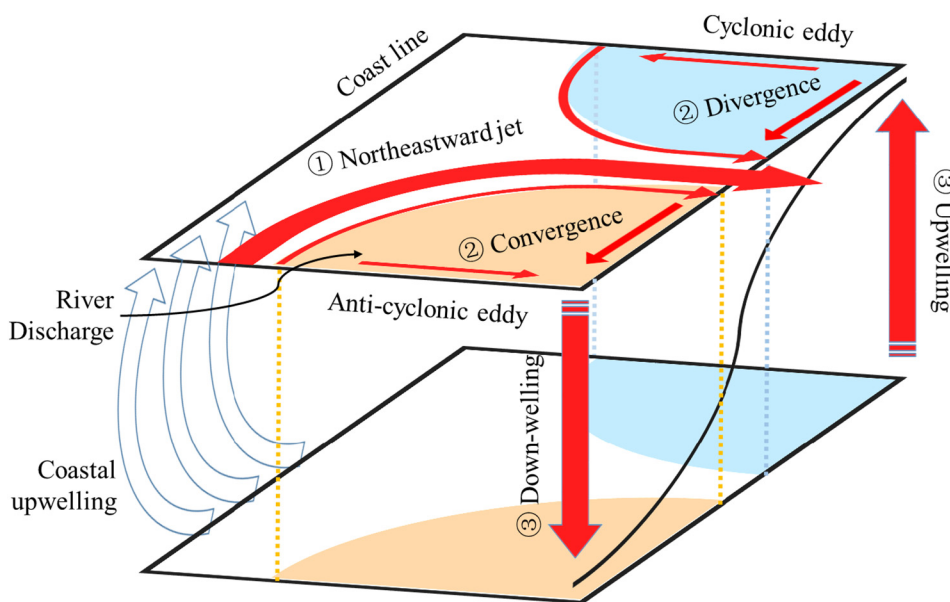


Fig. 10. Conceptual model of summertime ‘jet-eddies system’ in west South China Sea. Physical processes in the jet-eddies system include (1) horizontal advection by north-eastward jet, (2) divergence/convergence in cyclonic/anti-cyclonic eddy, and (3) upwelling/down-welling in cyclonic/anti-cyclonic eddy. (For interpretation of the references to color in this figure, the reader is referred to the web version of this article.)

upwelling water by the northeastward jet (Figs. 2 and 3c) supplied nutrients for the growth of phytoplankton. It is responsible for this distribution, similar to the description in Tang et al. (2004a) and Chen et al. (2014). Meanwhile, the vertical distribution of phytoplankton indicated that the northeastward jet influences not only the surface but also in the upper layer (< 25 m) of the open sea (Fig. 7).

The jet shaped patchiness between eddies was observed in anticyclonic circulation (Fig. 5) and performed similarly as other years (Tang et al., 2004b). This indicated that a larger volume of coastal water transported by the jet is prone to enter the anticyclonic area. Moreover, strong salinity variation showed in surface water between the northern and southern study regions, with a salinity front emerging at ~11°N in the coastal area and going northeastward to the open sea (Fig. 2b). Mekong river discharge was the main source of low-salinity water taking over the anticyclonic area in the south. On one hand, convergence formed the cap in the anticyclonic eddy. On the other hand, divergence may be responsible for the salinity front by uplifting deep water and restricting low salinity water out of the boundary of the cyclonic eddy.

Usually, the maximum chlorophyll a concentration appears from 50 m to 100 m with values between 0.1 µg L⁻¹ to 0.6 µg L⁻¹ in the SCS

(Wang and Tang, 2014). The total chlorophyll a concentration increased from 25 m to 50 m with increased nutrient concentration (dash line in Fig. 9), whereas it decreased under 50 m with NO_x⁻ and PO₄⁻ increasing, which was possibly due to reduced light intensity (solid line in Fig. 9). Station 12, at the center of the cyclonic eddy, exhibited the maximum chlorophyll a at 25 m with higher density (Fig. 7). Meanwhile, the maximum chlorophyll a concentrations of stations 21 and 22 in the anticyclonic eddy, appeared at 75 m. The difference in maximum chlorophyll a concentration in the subsurface can be ascribed to different nutrient supplies caused by variable vertical motion. Uplifting deep water with high nutrients in the cyclonic eddy can enhance phytoplankton growth in shallow depths. However, vertical physical processes were weak and negligible compared to the strong surface current, and may not significantly influence surface water.

Based on both in situ and satellite data, we found that phytoplankton distribution cannot be simply explained by the influence of the jet, especially under a scenario of three dimensional distribution. Therefore, the present study integrates the jet and associated eddies in the western SCS and terms it as a ‘jet-eddy system’. Physical processes in the jet-eddy system includes (1) horizontal advection by a north-eastward jet, (2) divergence/convergence in cyclonic/anticyclonic

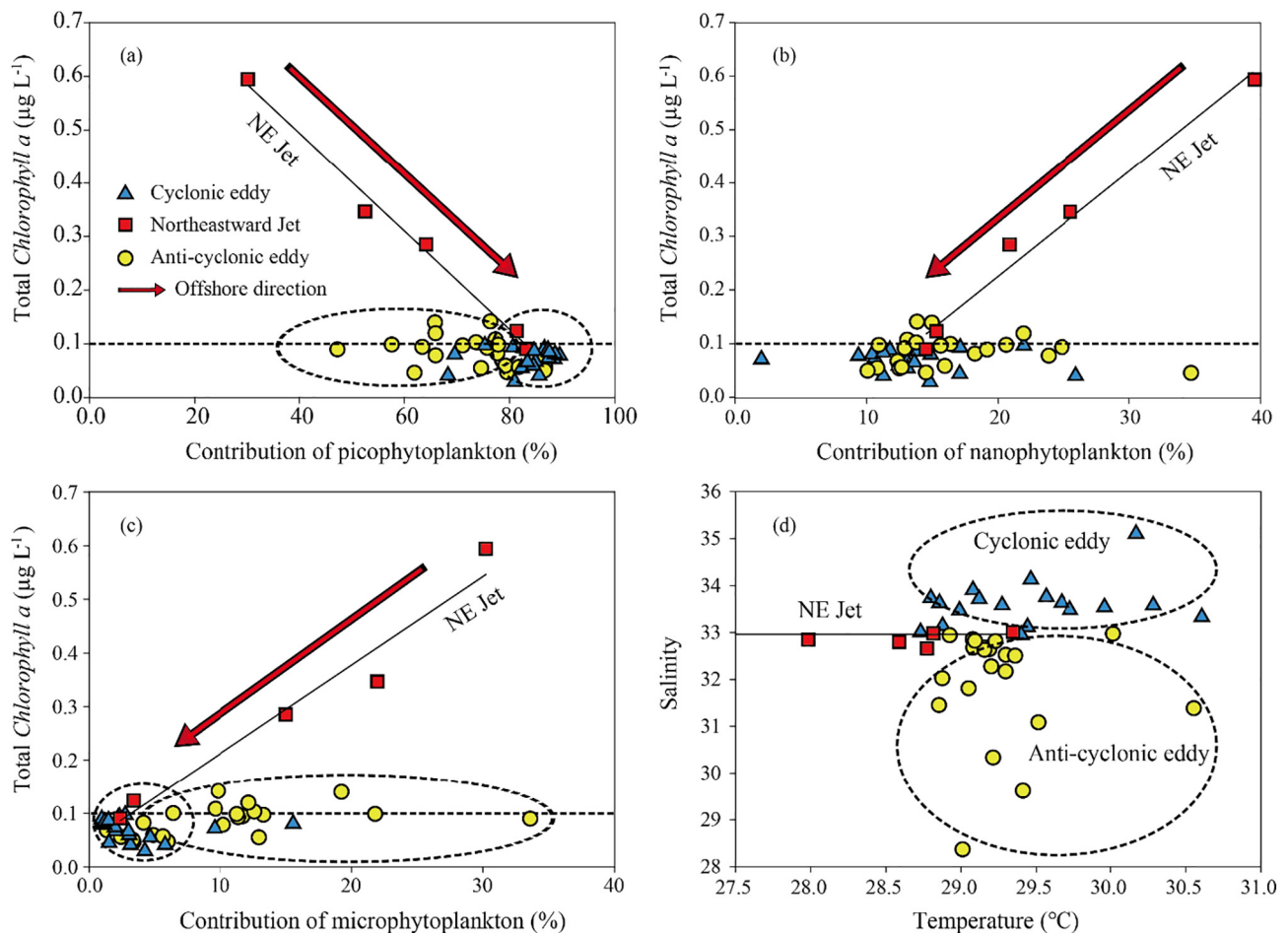


Fig. 11. Correlations between in situ sea surface total chlorophyll *a* and percentage of (a) picophytoplankton, (b) nanophytoplankton and (c) microphytoplankton. (d) Correlation between in situ surface temperature and salinity. Open triangles, filled squares and open circles represent stations in cyclonic ($SLA < -0.025$ m), northeastward jet (-0.025 m $< SLA < 0.025$ m) and anti-cyclonic ($SLA > 0.025$ m) area, respectively.

eddies, and (3) upwelling/down-welling in cyclonic/anticyclonic eddies (Fig. 10).

4.2. Physical processes of the jet-eddy system and their influence on phytoplankton size structure

Physical processes, such as advection, and changes in environmental variables such as temperature, solar radiation and nutrients are suggested to determine the PSS (Li, 2002; Finkel et al., 2009; Liu et al., 2009; Chen et al., 2010).

Microphytoplankton contributed over 20% of the total biomass at station 17 where the chlorophyll *a* concentration was high, but nutrients were low in the surface layer (Figs. 4 and 6e). Nutrient affinity to phytoplankton increased with decreasing body size (Donald et al., 1997). Picophytoplankton contributed more of the phytoplankton biomass in oligotrophic environments where nutrients are depleted ($\text{NO}_x < 1 \mu\text{M}$) (Agawin et al., 2000). In this case, low nutrients were possibly due to consumption by phytoplankton growth (Wang and Tang, 2014). Statistical analysis demonstrated a linear correlation between the percentage of all size fractions and the total chlorophyll *a* concentration in the northeastward jet area (red square in Fig. 10a–c). As the concentration decreases from the coast to the open sea, the contribution of micro- and nanophytoplankton showed a positive correlation with total chlorophyll *a* concentration, whereas the contribution of picophytoplankton was negative. This linear correlation indicated that horizontal advection of coastal upwelling water by the northeastward jet affected the surface PSS in the western SCS. Grosse et al.

(2010) observed that diatoms were the predominant group in the Mekong River Estuary during summertime. Diatoms, which prefer eutrophic and cooler environments, usually have a larger cell size than other phytoplankton groups (Glibert et al., 2016). The northeastward jet area showed lower temperature than the eddy regions (Fig. 11d and Table 1). Moreover, station 16, the first that the jet reached from land, was the unique station dominated by microphytoplankton. It had the lowest temperature among all sample stations, especially lower than station 15 which was at the same latitude but closer to land. This also suggested the strong jet influence. Therefore, the northeastward jet may not only supply nutrients to fuel the growth of phytoplankton, but create a cooler environment, especially for larger size phytoplankton such as the diatom group. However, the northeastward jet impact decreased with offshore distance. Reduced nutrients fertilized a higher rate of picophytoplankton growth, and thus enhanced the contribution of smaller phytoplankton to the total biomass.

The anticyclonic eddies exhibited a similar average chlorophyll *a* concentration in surface water, but with higher concentration and average percentage of microphytoplankton than the cyclonic eddy (Table 1 and Fig. 11c). Capped by the less-saline water, subsurface water was not able to reach the surface, and thus the nutrient supply from local deep water was limited (Fig. 11d). As discussed above, under the combined effect of divergence in the cyclonic eddy and convergence in the anticyclonic eddy, water mass from the northeastward jet with a higher proportion of larger phytoplankton was mainly delivered into the anticyclonic eddy area and diluted by the low salinity river plume, which resulted in the variation of size.

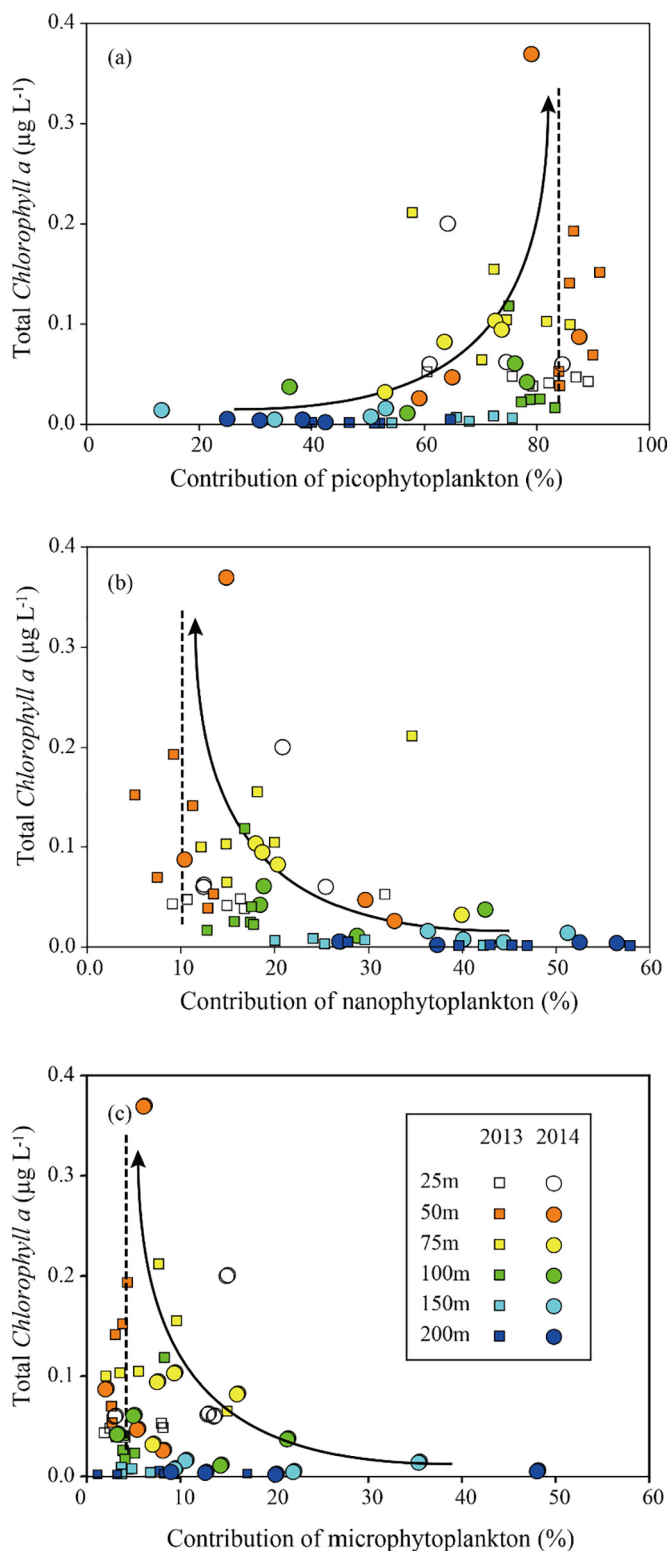


Fig. 12. Correlations between total *chlorophyll a* in subsurface layer of upper 200 m and contribution of (a) picophytoplankton, (b) nanophytoplankton and (c) microphytoplankton. Squares and circles represent sample collect from northeastern SCS (2013) and western SCS (2014).

In the subsurface layer, the vertical PSSs from the western SCS were compared to samples collected from the northeastern SCS in 2013. The PSS in both regions showed the same relation with *chlorophyll a* concentration. Phytoplankton at 25 m had a similar size structure to that at 50 m, where picophytoplankton was elevated, but the chlorophyll *a*

concentration was much less (Fig. 12). As *chlorophyll a* concentration declined from shallow (50 m) to deeper depth (200 m), the dominant phytoplankton size switched from pico to nano and micro (Fig. 12). This indicated that a *chlorophyll a* maximum layer may be a turning point to distinguish oligotrophic and eutrophic environments by PSS. In the depth above the *chlorophyll a* maximum layer, nutrients were depleted, which was favorable for picophytoplankton growth. Nevertheless, in the depth below the *chlorophyll a* maximum layer, increasing nutrients accelerated the growth rate of larger size phytoplankton, leading to the change in PSS.

However, station 30 in the cyclonic eddy presented a higher contribution of nano- and microphytoplankton than other stations at the same depth in the subsurface layer (blue circle in Fig. 13). Temperature and salinity data showed that the deeper water was uplifted to the upper 25 m in the cyclonic eddy area (Fig. 3). Nutrient profiles also indicated that nutrients increased in the vertical water column (Fig. 4). Both Zhong et al. (2013) and Wang et al. (2016) reported an increase of the diatom proportion of the phytoplankton community with bathymetry in the cyclonic eddy in the summertime western SCS. Therefore, upwelling in the cyclonic eddy can enhance nutrient supply, resulting in diatom growth and a higher contribution of larger phytoplankton. Meanwhile, station 24 in the anticyclonic eddy presented a strong depletion of nano- and microphytoplankton at depths of 25 m and 50 m (red circle in Fig. 13), which may be caused by limited nutrient supply from down-welling. The boost of *Synechococcus* and *Prochlorococcus* in the subsurface of anticyclonic eddies, observed by Zhong et al. (2013), indicated that this oligotrophic condition might induce the decline of larger sizes.

Generally, the PSS in the western SCS in summer can be well explained by the jet-eddy system. In the surface layer, horizontal advection by a northeastward jet and divergence/convergence in cyclonic/anticyclonic eddies (processes 1 and 2 in Fig. 10) were responsible for the distribution of PSS. However, in subsurface layers, nutrient variations induced by upwelling/down-welling in cyclonic/anticyclonic eddies (process 3 in Fig. 10) may affect the vertical PSS distribution.

4.3. Source water for jet-eddy system effects on phytoplankton biomass and its size structure

Previous studies illustrated that river influx delivered a huge amount of nitrogen to the sea, and could fertilize the marine ecosystem (Gan et al., 2010; Chen et al., 2011). In this study, the influence of river influx may be restricted in near-shore waters on the shallow shelf and the central part of the SCS is still oligotrophic with nutrient concentration below detection limits. The Mekong River plume was strongly depleted in nutrients due to mangrove forest consumption along the river, so phytoplankton was mainly fertilized by nutrient enriched upwelling water rather than nutrient depleted riverine water (Dippner et al., 2007).

Anticyclonic eddies were affected by the Mekong River discharge as evidenced by low salinity on the surface. Due to the convergence process, the surface of the anticyclonic eddy (yellow circle in Fig. 10d) was fed by diluted coastal water, exhibiting a lower salinity than the cyclonic eddy (blue triangle in Fig. 10d). Phytoplankton were mainly transported by the northeastward jet from coastal areas. Dilution of coastal water through convergence was responsible for similar *chlorophyll a* concentration but higher contribution of microphytoplankton in the anticyclonic eddy compared to the cyclonic eddy.

Meanwhile, the vertical contributions of nano- and microphytoplankton were strongly depleted at shallow depths in the anticyclonic eddy (Fig. 13). Influenced by down-welling in the anticyclonic eddy, the relatively fresh water strengthened the vertical density stratification and restricted the uplift of nutrients, resulting in a low contribution of larger size phytoplankton in the subsurface. Jyothibabu et al. (2015) indicated that a low salinity cap induced by the adjacent river significantly reduced the phytoplankton biomass and the

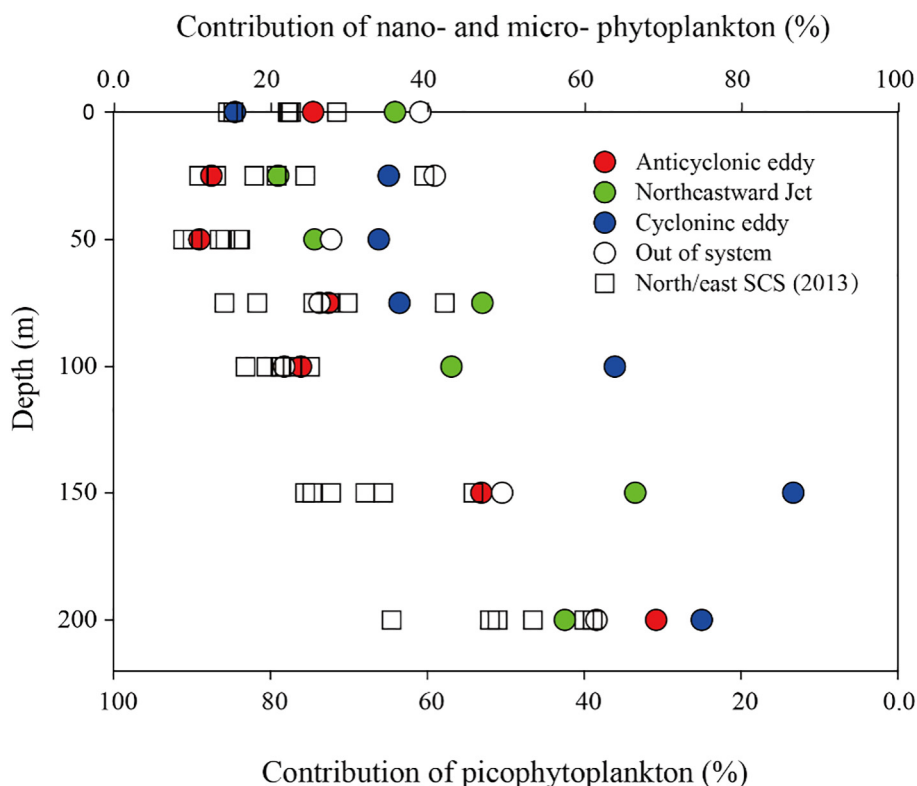


Fig. 13. Contribution of different size phytoplankton at different depths. Squares and circles represent sample collect from northeastern SCS (2013) and western SCS (2014). (For interpretation of the references to color in this figure, the reader is referred to the web version of this article.)

contribution of microphytoplankton in upper layer of the cyclonic eddy area, whereas nutrient enriched coastal upwelling water led to a phytoplankton bloom in subsurface layers due to the high contribution of microphytoplankton. Therefore, source water (riverine and coastal upwelling water), that feeds the jet-eddy system was considered to be another key factor affecting phytoplankton biomass and its size structure in the western SCS in summer.

5. Conclusion

The present study proposes a ‘jet-eddy system’ in the western SCS. Physical processes in the jet-eddy system include (1) horizontal advection by a northeastward jet, (2) divergence/convergence in cyclonic/anticyclonic eddies, and (3) upwelling/down-welling in cyclonic/anticyclonic eddies.

Generally, the ‘jet-eddy system’ determines the phytoplankton bloom and its size structure, though picophytoplankton dominates most of the western SCS in the summertime. In the surface layer, horizontal advection by the northeastward jet and divergence/convergence in cyclonic/anticyclonic eddies are responsible for the PSS and high microphytoplankton contribution in the jet and anticyclonic eddy. However, in subsurface water, nutrient supply and weakening of light intensity synergistically influence the concentration and size structure of phytoplankton in cyclonic/anticyclonic eddies at different depths. Source water (riverine and coastal upwelling water) that feeds the ‘jet-eddy system’ is another key factor affecting phytoplankton biomass and its size structure in the western SCS in summer.

Acknowledgement

This study was supported by National Natural Sciences Foundation of China (41430968) and Key project of Guangdong Institute for International Strategic (17ZDA24) awarded to Professor Danling Tang. The authors would like to thank Prof. Jiu Jimmy Jiao and Dr. Yi Liu

from the University of Hong Kong for their help when sampling in the field and testing, and thank to the open research cruise in northern South China Sea, 2013 and western South China Sea, 2014, supported by NSF.

References

- Agawin, N.S.R., Duarte, C.M., Agustí, S., 2000. Nutrient and temperature control of the contribution of picoplankton to phytoplankton biomass and production. *Limnol. Oceanogr.* 45 (3), 591–600.
- Chen, B.J., Liu, H.B., 2010. Relationships between phytoplankton growth and cell size in surface oceans: interactive effects of temperature, nutrients, and grazing. *Limnol. Oceanogr.* 55 (3), 965–972.
- Chen, W., Liu, Q., Huh, C.A., et al., 2010. Signature of the Mekong River plume in the western South China Sea revealed by radium isotopes. *J. Geophys. Res.-Atmos.* 115 (C12), 993–999.
- Chen, B., Wang, L., Song, S., et al., 2011. Comparisons of picophytoplankton abundance, size, and fluorescence between summer and winter in northern South China Sea. *Cont. Shelf Res.* 31 (14), 1527–1540.
- Chen, G., Xiu, P., Chai, F., 2014. Physical and biological controls on the summer chlorophyll bloom to the east of Vietnam. *J. Oceanogr.* 70 (3), 323–328.
- Cloern, J.E., 1996. Phytoplankton bloom dynamics in coastal ecosystems: a review with some general lessons from sustained investigations of San Francisco Bay, California. *Rev. Geophys.* 34 (2), 127–168.
- Dagg, M., Benner, R., Lohrenz, S., Lawrence, D., 2004. Transformation of dissolved and particulate materials on continental shelves influenced by large rivers: plume processes. *Cont. Shelf Res.* 24, 833–858. <http://dx.doi.org/10.1016/j.csr.2004.02.003>.
- Dippner, J.W., Nguyen, K.V., Hein, H., et al., 2007. Monsoon-induced upwelling off the Vietnamese coast. *Ocean Dyn.* 57 (1), 46–62.
- Donald, K.M., Scanlan, D.J., Carr, N.G., et al., 1997. Comparative phosphorus nutrition of the marine cyanobacterium *Synechococcus* WH7803 and the marine diatom *Thalassiosira weissflogii*. *J. Plankton Res.* 19 (12), 1793–1813.
- Finkel, Z.V., Vaillancourt, C.J., Irwin, A.J., et al., 2009. Environmental control of diatom community size structure varies across aquatic ecosystems. *Proc. R. Soc. B Biol. Sci.* 276 (1662), 1627–1634.
- Gan, J.P., Qu, T.D., 2008. Coastal jet separation and associated flow variability in the southwest South China Sea. *Deep-Sea Res. I Oceanogr. Res. Pap.* 55 (1), 1–19.
- Gan, J., Lu, Z.M., Dai, M.H., et al., 2010. Biological response to intensified upwelling and to a river plume in the northeastern South China Sea: a modeling study. *J. Geophys. Res. Oceans* 115 (C9), 292–295.
- Glibert, P.M., Wilkerson, F.P., Dugdale, R.C., et al., 2016. Pluses and minuses of ammonium and nitrate uptake and assimilation by phytoplankton and implications for

- productivity and community composition, with emphasis on nitrogen-enriched conditions. *Limnol. Oceanogr.* 61 (1), 165–197.
- Grosse, J., Bombar, D., Hai, N.D., Nguyen, L.N., Voss, M., 2010. The Mekong river plume fuels nitrogen fixation and determines phytoplankton species distribution in the South China Sea during low- and high-discharge season. *Limnol. Oceanogr.* 55 (4), 1668–1680.
- Hu, J., Kawamura, H., Hong, H., Qi, Y., 2000. A review on the currents in the South China Sea: seasonal circulation, South China Sea warm current and Kuroshio intrusion. *J. Oceanogr.* 56 (6), 607–624.
- Hu, J.Y., Gan, J.P., Sun, Z.Y., et al., 2011. Observed three-dimensional structure of a cold eddy in the southwestern South China Sea. *J. Geophys. Res. Oceans* 116 (C5), 86.
- Huang, B.Q., Hu, J., Xu, H.Z., et al., 2010. Phytoplankton community at warm eddies in the northern South China Sea in winter 2003/2004. *Deep-Sea Res. II Top. Stud. Oceanogr.* 57 (19–20), 1792–1798.
- Irwin, A.J., 2006. Scaling-up from nutrient physiology to the size-structure of phytoplankton communities. *J. Plankton Res.* 28 (5), 459–471 (13).
- Jyothibabu, R., Vinayachandran, P.N., Madhu, N.V., et al., 2015. Phytoplankton size structure in the southern Bay of Bengal modified by the Summer Monsoon Current and associated eddies: implications on the vertical biogenic flux. *J. Mar. Syst.* 143, 98–119.
- Kuo, N.J., Zheng, Q., Ho, C.R., 2000. Satellite observation of upwelling along the western coast of the South China Sea. *Remote Sens. Environ.* 74 (3), 463–470.
- Li, W.K.W., 2002. Macroecological patterns of phytoplankton in the northwestern North Atlantic Ocean. *Nature* 419 (6903), 154–157.
- Li, Y., Han, W., Wilkin, J.L., Zhang, W.G., et al., 2014. Interannual variability of the surface summertime eastward jet in the South China Sea. *J. Geophys. Res. Oceans* 119 (10), 7205–7228.
- Lin, I.I., Lien, C.C., Wu, C.R., et al., 2010. Enhanced primary production in the oligotrophic South China Sea by eddy injection in spring. *Geophys. Res. Lett.* 37 (16), 127–137.
- Liu, C.L., Tang, D.L., Wang, S.F., et al., 2009. Variations in the dominant algal bloom-forming species in the western South China Sea from 1993 to 2007. *Afr. J. Mar. Sci.* 31 (3), 373–380.
- McGillicuddy, D.J., Anderson, L.A., Doney, S.C., Maltrud, M.E., 2003. Eddy-driven sources and sinks of nutrients in the upper ocean: results from a 0.1 resolution model of the North Atlantic. *Glob. Biogeochem. Cycles* 17 (2).
- Ning, X., Chai, F., Xue, H., et al., 2004. Physical-biological oceanographic coupling influencing phytoplankton and primary production in the South China Sea. *J. Geophys. Res. Oceans* 109 (10), 215–255.
- Ryther, J.H., 1969. Photosynthesis and fish production in the sea. The production of organic matter and its conversion to higher forms of life vary throughout the world ocean. *Science (Washington)* 166, 72–76.
- Shaw, P.T., Chao, S.Y., 1994. Surface circulation in the South China Sea. *Deep-Sea Res. I Oceanogr. Res. Pap.* 41 (11–12), 1663–1683.
- Sun, Q., Tang, D.L., Legendre, L., Shi, P., 2014. Enhanced sea-air CO₂ exchange influenced by a tropical depression in the South China Sea. *J. Geophys. Res. Oceans* 119, 6792–6804. <http://dx.doi.org/10.1002/2014JC010131>.
- Tang, D.L., Kawamura, H., Hai, D.N., et al., 2004a. Remote sensing oceanography of a harmful algal bloom off the coast of southeastern Vietnam. *J. Geophys. Res.-Atmos.* 109 (C3), 325–347.
- Tang, D.L., Kawamura, H., Dien, T.V., et al., 2004b. Offshore phytoplankton biomass increase and its oceanographic causes in the South China Sea. *Mar. Ecol. Prog. Ser.* 268 (1), 31–41.
- Tang, D.L., Hiroshi, K., Ping, S., et al., 2006. Seasonal phytoplankton blooms associated with monsoonal influences and coastal environments in the sea areas either side of the Indochina Peninsula. *J. Geophys. Res. Biogeosci.* 111 (G1), 355–363.
- Vaillancourt, R.D., Marra, J., Seki, M.P., et al., 2003. Impact of a cyclonic eddy on phytoplankton community structure and photosynthetic competency in the subtropical North Pacific Ocean. *Deep-Sea Res. I Oceanogr. Res. Pap.* 50 (7), 829–847.
- Voss, M., Bombar, D., Loick, N., Dippner, J.W., 2006. Riverine influence on nitrogen fixation in the upwelling region off Vietnam, South China Sea. *Geophys. Res. Lett.* 33 (7).
- Wang, J.J., Tang, D.L., 2014. Phytoplankton patchiness during spring intermonsoon in western coast of South China Sea. *Deep-Sea Res. I Oceanogr. Res. Pap.* 101 (3), 120–128.
- Wang, G.H., Chen, D., Su, J.L., 2006. Generation and life cycle of the dipole in the South China Sea summer circulation. *J. Geophys. Res. Oceans* 111 (C6), 161–173.
- Wang, L., Huang, B., Chiang, K.P., et al., 2016. Physical-biological coupling in the western South China Sea: the response of phytoplankton community to a mesoscale cyclonic eddy. *PLoS One* 11 (4), e0153735.
- Xie, S.P., Xie, Q., Wang, D.X., et al., 2003. Summer upwelling in the South China Sea and its role in regional climate variations. *J. Geophys. Res. Oceans* 108 (C8), 343–367.
- Ye, H., Sheng, J., Tang, D., Siswanto, E., Ali Kalhor, M., Sui, Y., 2017. Storm-induced changes in pCO₂ at the sea surface over the northern South China Sea during Typhoon Wutip. *J. Geophys. Res. Oceans* 122, 4761–4778. <http://dx.doi.org/10.1002/2016JC012643>.
- Zhong, C., Xiao, W.P., Huang, B.Q., 2013. The response of phytoplankton to mesoscale eddies in western South China Sea. *Adv. Mar. Sci.* 31 (2), 213–220 (in Chinese).